Stability Criterion for the Assembly of Hybrid Lipid-Polymer-Nucleic Acid Nanoparticles

Juan L. Paris[1, *], Ricardo Gaspar[1], Filipe Coelho[1], Pieter A. A. De Beule[1], Bruno F. B. Silva[1, *]

[1]International Iberian Nanotechnology Laboratory, Av. Mestre José Veiga, Braga, Portugal

*Corresponding authors: juan.paris@ibima.eu, bruno.silva@inl.int

Abstract: Hybrid lipid-polymer-nucleic acid nanoparticles (LPNPs) provide unique delivery strategies for nonviral gene therapy. Since LPNPs consist of multiple components that can undergo different pairwise interactions between them, LPNPs are difficult to prepare and characterize. Here we demonstrate that the interaction between the polycation (polylysine) and DNA is robust through an innovative implementation of fluorescence cross-correlation spectroscopy, implying that the polycation is not displaced by cationic liposomes in the formation process. Hence, the polycation-DNA cores (polyplexes) and liposome shells must be oppositely charged to associate. Furthermore, we prove that the liposome:polyplex number ratio (ρ_N) is the primary critical parameter to predict stable LPNP formation. We establish that $\rho_N \geq 1$ is required to ensure that every polyplex is enveloped by a liposome, avoiding the coexistence of oppositely charged species and thereby inhibiting aggregation. We expect our observations to be valid for the formation of many other LPNPs and composite nanomaterials.

Keywords: Lipopolyplex, Lipid-polycation-DNA (LPD), gene delivery, fluorescence cross-correlation spectroscopy, FCCS.

1. INTRODUCTION

Non-viral gene delivery to treat genetic and acquired diseases has become clinical reality through the introduction of an siRNA-based treatment for hereditary transthyretin-mediated amyloidosis[1] and lipid-based mRNA vaccines to address the COVID-19 pandemic[2,3]. Further applications in the pipeline encompass the development of personalized cancer vaccines[4–6] and permanent knockout of defective genes using CRISPR/Cas9 technology[7]. Most nonviral gene formulations reaching the clinic rely on the use of ionizable cationic lipid formulations as nanocarriers. These materials readily associate with the oppositely charged nucleic acids (NAs), embedding them into internally structured nanoparticles that can be therapeutically efficient *in vivo*[1,8–12]. Notwithstanding this success, the efficacy of non-viral gene therapies remains limited in many cases, particularly for therapeutic targets beyond the liver and immune cells[13]. A promising approach to endow nanocarriers with higher functionality to overcome the many physiological barriers to gene delivery[14–16] consists in the use of hybrid lipid-polycation-nucleic acid nanoparticles (LPNPs)[17–25]. These nanomaterials consist of a core composed by polycations complexed with NAs (i.e. polyplexes[26]), enveloped by a lipid membrane (Figure 1a). Since the polyplex core and

shell components can be independently designed, functionality can be improved[17], for example through an outer lipid membrane designed for cell-specific targeting and a polycation core optimized for endosomal escape[27].

LPNPs are complex to produce and characterize since multiple pairwise interactions need to be considered: polycation-DNA, liposome-DNA and liposome-polycation. Typically, the core polyplex is formed first, followed by the addition of oppositely charged liposomes that drive electrostatic complexation between both species, reminiscent of electrostatic-based layer-by-layer assembly[28]. Alternative structures to core-shell LPNPs may form when the polycation and cationic lipids are added to the nucleic acids simultaneously[29,30], but even when added sequentially, competing interactions between the tree components can still drive the formation of other structures and displace one of the components (Figure 1a).

Elucidating the critical interactions in the LPNP formation process is challenging with widely applied techniques such as Dynamic Light Scattering (DLS), Electrophoretic Mobility, and Transmission Electron Microscopy (TEM). We add dual-colour Fluorescence Cross-Correlation Spectroscopy (FCCS)[31–33] to this toolset to quantitatively assess the extent of association between polyplexes and liposomes in the formation of LPNPs. The incorporation of FCCS in the standard characterization toolset of other composite materials involving hierarchical assembly is likely to bring further innovation.

2. RESULTS AND DISCUSSION

2.1. Size and $\zeta_{\mathrm{Potential}}$ reveal stability regions and hint at LPNP formation.

A series of samples with varying ratios between lipids, polycations and DNA was prepared to study LPNP assembly behaviour. Sample compositions are defined through the molar ratios of cationic lipids in the liposomes ($\rho_{\mathrm{L:DNA}}$) and ionizable-cationic amine groups in the polycations ($\rho_{\mathrm{P:DNA}}$), to anionic groups in DNA. Polylysine, a common cationic polymer in both polyplex and LPNP systems[34,35], was chosen as polycation, and its concentration fixed at 7 μg/ml. A lipid mixture of DOTAP:DOPC:PEG2K was used for liposome preparation, whereby the cationic lipid DOTAP was maintained in a fixed amount (80 mol%) alongside varying amounts of PEG-lipid.

The methodology for assembling LPNPs is shown in Figure 1a. A polyplex core is assembled in a preliminary step by mixing polylysine with DNA at a fixed $\rho_{\mathrm{P:DNA}}$ ratio of 1, 1.5 and 3. Subsequently, cationic liposomes are added to form core-shell LPNPs. The isoelectric point (ρ_{iso}) between polylysine and DNA was determined to be 1.6[36]. $\rho_{\mathrm{P:DNA}} = 1$ polyplexes are negatively overcharged with DNA, showing a negative $\zeta_{\mathrm{Potential}}$ (Figure 1b) and are likely to also contain a significant fraction of non-

complexed DNA in excess[34]. $\rho_{\mathrm{P:DNA}} = 1.5$ polyplexes are close to the ρ_{iso}, showing a smaller negative $\zeta_{\mathrm{Potential}}$ and are likely to contain just a minute amount of non-complexed DNA, if any. Conversely, $\rho_{\mathrm{P:DNA}} = 3$ polyplexes are cationic, and virtually all the DNA is expected to be complexed, coexisting with excess polycations. The size of the polyplexes varies with $\rho_{\mathrm{P:DNA}}$, being all smaller than 140 nm (Figure 1c). The cationic liposomes presented a hydrodynamic diameter (D_H) of ca. 100 nm and high $\zeta_{\mathrm{Potential}}$ values (Table S2 of the supplementary information, SI). The $\zeta_{\mathrm{Potential}}$ and size results for the LPNP formulations are shown in figure 1b-1c. The complete set of data including polydispersity index (PDI) can be found in Table S3.

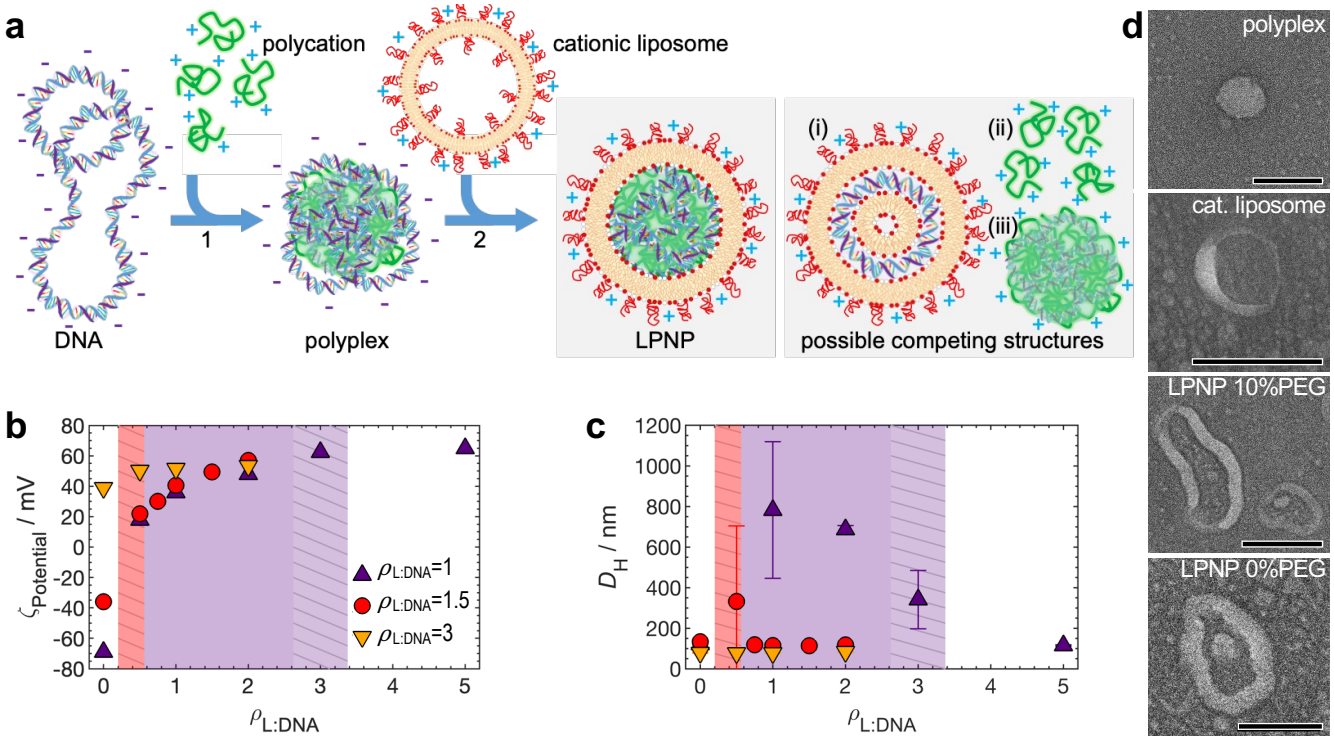

Figure 1. Lipid-Polymer hybrid nanoparticle (LPNP) assembly and physical properties. (**a**) Schematic illustration of the LPNP assembly strategy, consisting of a preliminary step (1) where DNA and polycations are mixed to form polyplexes with an excess negative charge, and a second step (2) where polyplexes are mixed with oppositely charged cationic liposomes to form LPNPs. Along with (or instead of) LPNP formation, hypothetical competing structures can form, such as lipid-DNA complexes (i), polycations released from the polyplex core (ii) or positively charged polyplexes striped from the outer DNA layers (iii). (**b**) ζ potential and (**c**) hydrodynamic diameter (D_H) of the three LPNP systems as a function of $\rho_{\mathrm{L:DNA}}$. The red dashed area represents the region of the $\rho_{\mathrm{P:DNA}}$=1.5 system where aggregation was observed in some samples. The purple area represents the region of the $\rho_{\mathrm{P:DNA}}$=1 system where large aggregation was observed, and the purple dashed area represents the region where aggregation was observed only in some samples. Data are Means ± SD (n=3). (**d**) TEM images of polyplexes, liposomes and LPNPs with 10 and 0 mol% PEG.

Figure 1b-1c indicates two trends for the LPNP systems depending on the surface charge of the starting polyplex. For samples obtained from cationic polyplexes ($\rho_{\mathrm{P:DNA}} = 3$) neither size nor $\zeta_{\mathrm{Potential}}$ are significantly affected when cationic liposomes are added. Conversely, when the starting polyplex presents negative $\zeta_{\mathrm{Potential}}$ ($\rho_{\mathrm{P:DNA}} = 1$ and 1.5), LPNP charge switches to cationic already at the lowest $\rho_{\mathrm{L:DNA}}$ additions, coinciding with the observation of strong aggregation ($D_H > 500\mathrm{nm}$), especially for $\rho_{\mathrm{P:DNA}} = 1$. Further addition of liposomes leads to stabilization. Clear solutions with $D_H < 120\mathrm{nm}$ are obtained for $\rho_{\mathrm{L:DNA}} = 5$ and $\rho_{\mathrm{L:DNA}} = 0.75$ for $\rho_{\mathrm{P:DNA}} = 1$ and $\rho_{\mathrm{P:DNA}} = 1.5$ LPNPs, respectively. Since $\rho_{\mathrm{P:DNA}} = 1$ polyplexes are more negatively charged and are expected to coexist with significant amounts of free DNA in solution (which needs to be neutralized), more liposomes are needed to stabilize these LPNPs when compared with the $\rho_{\mathrm{P:DNA}} = 1.5$ system. Yet, at a first glance, the factor of ca. six times larger $\rho_{\mathrm{L:DNA}}$ needed to stabilize $\rho_{\mathrm{P:DNA}} = 1$ polyplexes seems high. TEM results (Figure 1d) confirm the formation of LPNPs, with imaged particles showing a core like the polyplex samples, enveloped by a membrane.

Negative polyplexes aggregating initially and then redispersing for increasing $\rho_{\mathrm{L:DNA}}$ hints at strong electrostatic interactions with liposomes and conversion of polyplexes into LPNPs. One should however also consider other interactions potentially leading to the formation of structures competing with LPNPs (Figure 1a). For instance, DNA could be partially or entirely displaced from the polycation to the cationic liposomes to form lipoplexes. Such structures could have sizes and $\zeta_{\mathrm{Potential}}$ like LPNPs. Regarding the positively charged polyplexes ($\rho_{\mathrm{P:DNA}} = 3$), the lack of observable changes with $\rho_{\mathrm{L:DNA}}$ could hint at no formation of LPNPs, but also here one should consider the possibility of cationic liposomes displacing some polycations to form LPNPs. These alternative scenarios are difficult to discern with DLS/electrophoretic mobility and even with TEM.

2.2. Dual-colour fluorescence time traces provide semi-quantitative colocalization between cationic liposomes and polyplexes.

Colocalization between two entities labelled with two distinct fluorophores can be assessed qualitatively by looking at the spatial overlap between the two labels using fluorescence microscopy[22]. However, this approach is challenging to render quantitative[37]. FCCS can overcome this limitation and provide a quantitative measure of colocalization along with simultaneous determination of the sizes of the labelled species[31,32]. FCCS has been successfully used to characterize interactions between biologic species[31,32,38,39], and to assess the formation[33,40] (and disassembly[41]) of cationic liposome-DNA complexes, polymeric[42] and silica[43,44] nanoparticles, and liposome-coated metal organic frameworks[45].

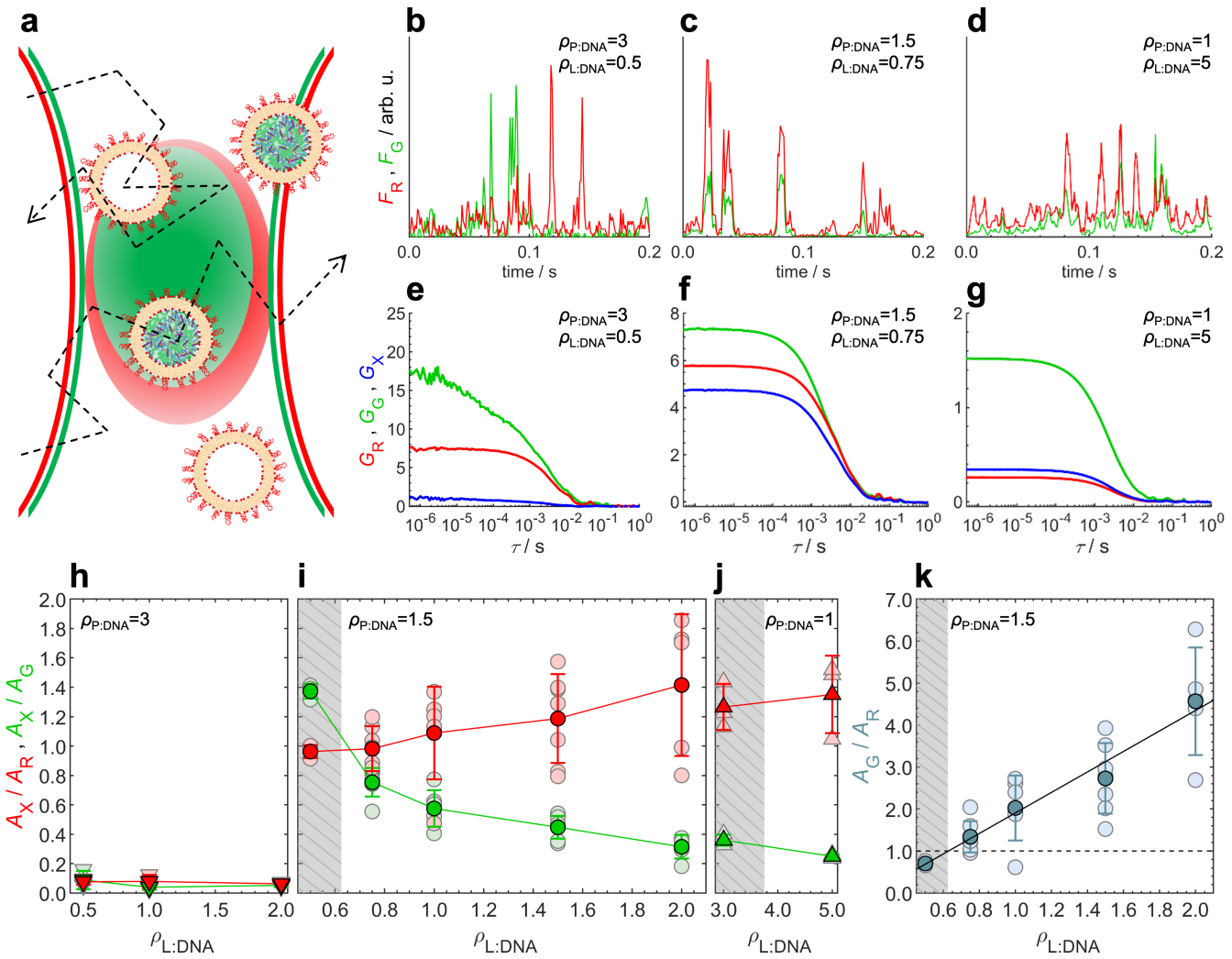

Figure 2. FCCS quantifies association between cationic liposomes and polyplexes. (**a**) Schematic illustration of the green and red confocal volumes with LPNPs and cationic liposomes diffusing through them. Panels **b-d** show representative fluorescence time traces for samples $\rho_{P:DNA}$=3, $\rho_{L:DNA}$=0.5; $\rho_{P:DNA}$=1.5, $\rho_{L:DNA}$=0.75; and $\rho_{P:DNA}$=1, $\rho_{L:DNA}$=5, respectively. Panels **e-g** show the corresponding auto and cross-correlation curves for the same samples. The green and red fluorescence (F_G and F_R) and auto-correlation curves (G_G and G_R) are shown in green and red, respectively. The cross-correlation curves ($G_{X.meas}$) are shown in blue. Non-associating particles, like cationic polyplexes and cationic liposomes, diffuse independently, producing uncorrelated green and red fluorescence fluctuations, visible both in the time traces (**b**) and in the negligeable amplitude of $G_{X.meas}$. in (**e**). LPNPs, containing both a polyplex (labelled with Atto488, green) and a cationic liposome (Texas-Red) produce correlated green and red fluorescence fluctuations, visible both in the time traces (**c** and **d**), and large amplitudes of $G_{X.meas}$ (**f** and **g**). Panels **h-j**, show the A_X/A_R (red symbols) and A_X/A_G (green symbols) ratios, which provide the fraction of polyplexes converted to LPNPs and the fraction of liposomes used in LPNPs, respectively. Individual measurements are represented by light-red and light-green symbols, while their means and respective error bars are represented by dark-red and dark-green. A_X/A_R and A_X/A_G are very low for the $\rho_{P:DNA}$=3 system, confirming negligeable association between polyplexes and liposomes with the same charge sign (**h**). The A_X/A_R ratio for $\rho_{P:DNA}$=1.5 (**i**) and $\rho_{P:DNA}$=1 (**j**) systems is ≈1 for low $\rho_{L:DNA}$ and increases slightly as $\rho_{L:DNA}$ increases, indicating full conversion of polyplexes to LPNPs, and an average number of liposomes per LPNP increasing slightly beyond one with $\rho_{L:DNA}$.

Conversely, A_X/A_G decreases steadily with $\rho_{L:DNA}$, indicating that after colloidal stability is reached, most added liposomes are in excess, not associating with LPNPs. Panel **k** shows the A_G/A_R ratio (for $\rho_{P:DNA}$=1.5), which is equivalent to the liposome:polyplex ratio (ρ_N) . The region of robust colloidal stability for LPNPs shows ρ_N>1. The region of marginal stability shows ρ_N<1. This suggests that $\rho_N \geq 1$ is a requirement for robust stability. The boundary between marginal and robust stability (ρ_N=1) is estimated at $\rho_{L:DNA}$=0.63 for $\rho_{P:DNA}$=1.5. The grey-dashed areas in **h**-**k** delineate the compositions of marginal stability, in which some samples were not measurable due to the presence of aggregates. Data are Means ± SD (n≥3).

To monitor the formation of LPNPs (Figure 1a), we label polylysine covalently with Atto-488 and likewise the cationic liposomes with Texas Red. Since both labelled species are cationic, they can only associate if DNA acts as an intermediary. Hence, colocalization between polylysine and liposomes indicates association between the liposomes and polyplex cores. Simultaneously, this rules out other competing structures in which DNA would be displaced, as illustrated in Figure 1a. If DNA is labelled instead of polycations, the absence of cross-correlation between both signals still discards the presence of LPNPs, but its presence does not allow for the distinction between LPNPs and other competing structures (e.g., lipoplexes). In the case of formulations starting with cationic polyplexes ($\rho_{\mathrm{P:DNA}} = 3$), the existence of labelled polycation free in solution makes the FCCS measurements difficult to analyse, and in this case the initial measurements were complemented with measurements whereby the DNA is labelled (YOYO-1, green) instead of the polycation.

In FCCS, the confocal volumes defined by the green and red lasers of a confocal microscope are fixed in space, while labelled species diffuse in and out of the overlapping green and red region (Figure 2a). If polyplexes and liposomes do not form LPNPs, they diffuse independently, producing uncorrelated spikes in the two fluorescence signals. This is the case for formulations starting with $\rho_{\mathrm{P:DNA}} = 3$ polyplexes, in which polyplexes and cationic liposomes show unsynchronized spikes in the fluorescence channels (Figure 2b). In contrast, if polyplexes and liposomes form LPNPs, they diffuse together producing correlated fluorescence signals. This is the case for the formulations starting with $\rho_{\mathrm{P:DNA}} = 1.5$ polyplexes (Figure 2c), where excellent overlap between the green and red signals is observed. For formulations starting with $\rho_{\mathrm{P:DNA}} = 1$ (Figure 2d), the spikes in the green channel overlap with red spikes, but there are many red spikes that have no overlap with green. This is because a high excess of liposomes is present, producing only red spikes. Overall, even if somewhat qualitative, these observations confirm LPNP formation when the charge is being inverted ($\rho_{\mathrm{P:DNA}} = 1$ and 1.5), but not when the charge of polyplexes and liposomes has the same sign ($\rho_{\mathrm{P:DNA}} = 3$).

2.3. FCCS auto- and cross-correlation quantify association between cationic liposomes and polyplexes.

For a quantitative analysis, the auto- and cross-correlation curves (resulting from time traces) can be examined[31,33] (Figures 2e-g). The green and red auto-correlation curves describe the dynamics of species carrying the green and red labels, respectively. Importantly, the cross-correlation curve results from the correlation between the two signals and therefore only contains information on the species carrying both labels. The decay time constants of these curves are related with the species' diffusion coefficients (Eqs. S2-S3) and are used to extract LPNP size (Table S4 and Figure S1). The amplitudes of the correlation curves contain information on the number of each labelled specie, and on the number of species containing both labels[31,37]. Hence, the fraction of LPNP formation can be determined. For the simplified case of: (i) one polyplex associating with one cationic liposome (1:1 stoichiometry) to form one LPNP; (ii) no crosstalk between the two channels; and (iii) no changes in the brightness of the species following the association, the equations relating the amplitudes of the correlation curves with the number of species in the confocal volume become straightforward (Eqs 1a-c).

$$A_G = \left(N_{\mathrm{PP}f} + N_{\mathrm{LPNP}}\right)^{-1} \tag{1a}$$

$$A_R = \left(N_{\mathrm{L}f} + N_{\mathrm{LPNP}}\right)^{-1} \tag{1b}$$

$$A_X = \frac{N_{\mathrm{LPNP}}}{\left(N_{\mathrm{PP}f} + N_{\mathrm{LPNP}}\right) \cdot \left(N_{\mathrm{L}f} + N_{\mathrm{LPNP}}\right)} \tag{1c}$$

Here, A_G and A_R are the amplitudes of the green and red auto-correlation, respectively, and A_X is the amplitude of the cross-correlation. N_{PPf}, N_{Lf}, and N_{LPNP}, are the average number of free polyplexes, free liposomes and LPNPs in the confocal volumes, respectively. The ratio between A_X and A_R provides a direct measure of the fraction of polyplexes that were converted to LPNPs (f_{LPNP}), according to:

$$A_X/A_R = N_{\mathrm{LPNP}}/\left(N_{\mathrm{PP}f} + N_{\mathrm{LPNP}}\right) = f_{LPNP} \tag{2a}$$

Conversely, the A_X/A_G ratio provides a direct measure of the fraction of cationic liposomes used to make LPNPs:

$$A_X/A_G = N_{\mathrm{LPNP}}/\left(N_{\mathrm{L}f} + N_{\mathrm{LPNP}}\right) \tag{2b}$$

The approximations above are reasonable since the experimental conditions are such that the crosstalk from the green to the red channel is kept low at ca. 10%, allowing for its correction[46], and the brightness of polyplexes and liposomes do not change significantly upon association. In section S2 of the SI we detail

why the 1:1 stoichiometry assumption is appropriate to estimate f_{LPNP} and a much more complex model based on 1:*n* stoichiometry with *n* liposomes per LPNP is not required.

The overlap volume correction factor ($V_{crct} = 74.6\%$), is determined in a controlled experiment using mixtures of single-labelled and double-labelled PEGylated liposomes (section S3 and Figure S3)[47]. After correcting the crosstalk[46], the A_X used in Eqs. 1-2 is obtained from the measured amplitude of the cross-correlation ($A_{X.meas}$) and V_{crct} according to:

$$A_X = A_{X.meas.}/V_{crct} \quad (3)$$

2.4. Liposomes and polyplexes with the same charge do not associate.

Starting with the $\rho_{\mathrm{P:DNA}} = 3$ system, where we had seen low synchronization between the green and red signals, Figure 2e shows that the amplitude of the cross-correlation curve $A_{X.meas.}$ is much lower than the amplitudes of the autocorrelation curves, resulting in A_X/A_R and A_X/A_G ratios very close to zero (Figure 2h). As mentioned above, in this $\rho_{\mathrm{P:DNA}} = 3$ case, the DNA was labelled instead of the polycation, but the absence of cross-correlation still proves lack of association between polyplexes and liposomes and virtually no LPNP formation. The correlation curves with polycations labelled instead are shown in Figure S4.

Like-charged polyplexes and liposomes are unlikely to associate unless there is a strong non-electrostatic interaction between them, or the liposomes replace part of the polycation in the polyplexes. Notwithstanding, some systems composed by cationic polyplexes and cationic liposomes have reported better transfection than the polyplexes alone[48]. It is unclear if in such cases the use of weaker polycations (e.g., polyethyleneimine – PEI) can lead to partial replacement of the polymer by liposomes to form LPNPs or if the presence of liposomes can boost transfection of polyplexes even without LPNP formation.

2.5. Oppositely charged liposomes and polyplexes near ρ_{iso} associate strongly

In contrast with cationic polyplexes, the $\rho_{\mathrm{P:DNA}} = 1.5$ system shows a much larger $A_{X.meas.}$, comparable to both A_G and A_R, indicating strong colocalization (Figure 2f). Since in this case, both labelled species are cationic (polycation with green and liposomes with red), their colocalization indicates strong association between polyplexes and liposomes.

Figure 2i, shows the corrected A_X/A_R and A_X/A_G ratios as a function of $\rho_{\mathrm{L:DNA}}$. It is noticeable that while the mean values present well-defined and robust trends, the individual measurements (typically five-six independent samples) are significantly noisier, especially A_X/A_R. This occurs because FCCS operates in a quasi-single-particle regime, requiring long measurement times or multiple measurements to reach

adequate statistics. Since long measurements are not feasible due to sample drying, shorter measurements were performed with several independently prepared samples, exhibiting a larger variability that vanishes when computing the mean. Note also that while the variability of A_X/A_R is significant, the variability of A_X/A_G is much lower. This is expected if most polyplexes are converted to LPNPs coexisting with excess liposomes. The apparently noisier nature of the individual measurements is therefore not of concern, as can be also confirmed by the results of LPNPs assembled with 0 and 5% PEG liposomes, which show the same trends—noisy individual A_X/A_R measurements, but robust means with well-defined trends (Figure 3a).

Within the 1:1 liposome:polyplex stoichiometry ratio approximation A_X/A_R is equal to f_{LPNP} (Eq 2a). It is noticeable that A_X/A_Rincreases from ca. 1 to 1.42 as $\rho_{\mathrm{L:DNA}}$ is increased from 0.5 to 2. This indicates a practically full conversion of polyplexes into LPNPs (f_{LPNP}≈1) in detriment of the alternative structures depicted in Figure 1a. The fact that the average A_X/A_R values become larger than one for higher $\rho_{\mathrm{L:DNA}}$ indicates that for larger amounts of added liposomes, some LPNPs may have two liposomes attached, resulting in a 1:*n* stoichiometry with *n* slightly greater than 1, but still with f_{LPNP}≈1. A more detailed analysis considering the 1:*n* stoichiometry is provided in section S2, confirming f_{LPNP}≈1. Under such conditions *n*~1.7 for $\rho_{\mathrm{L:DNA}} = 2$, which indicates that even at the largest $\rho_{\mathrm{L:DNA}}$, most LPNPs will be associated with either one or two liposomes, and most liposomes added will be in excess.

Figure 2i also shows the A_X/A_G ratio, which directly provides the fraction of liposomes used to make LPNPs (Eqs 3b). A_X/A_G is greater than one for $\rho_{\mathrm{L:DNA}} = 0.5$, which suggests that for the smallest $\rho_{\mathrm{L:DNA}}$ there may not be enough liposomes to completely coat the polyplexes. This helps explaining why in this composition LPNP solutions are sometimes colloidally unstable. As $\rho_{\mathrm{L:DNA}}$ is increased, A_X/A_G starts to steadily decrease, indicating that there is now an excess of liposomes in solution that do not associate with the polyplexes. This supports a 1:*n* stoichiometry in which *n* is relatively close to one.

2.6. FCCS reveals that the liposome:polyplex number ratio ρ_N is the critical parameter determining stable LPNP formation, not the charge ratio.

In the previous section it became apparent that the ratio between the number of liposomes and polyplexes (ρ_N) is important. This quantity is not straightforward to obtain with most techniques but is easily accessible using FCCS. The total number of polyplexes and liposomes in solution is obtained through A_G^{-1} and A_R^{-1}, respectively (Eqs 1a-b). If n≈1, the A_G/A_R ratio then provides ρ_N. (Since n≈1.7 mostly when there are also many free liposomes, this results in a small error.)

Figure 2k shows that for the $\rho_{\mathrm{P:DNA}} = 1.5$ system, all the samples in the stable region ($\rho_{\mathrm{L:DNA}} \geq 0.75$) have a ρ_N ratio greater than one. Conversely, the samples in the marginally stable region ($\rho_{\mathrm{L:DNA}} = 0.5$) show a ρ_N slightly below one. This provides a very strong hint that $\rho_N \geq 1$ is a critical requirement to obtain robust colloidal stability.

If the number of liposomes is smaller than the number of polyplexes, some polyplexes will be transformed into cationic LPNPs while some others will remain anionic. Hence, even in a situation of large overall positive charge, if $\rho_N < 1$ the interactions between non-converted anionic polyplexes and converted cationic LPNPs can lead to aggregation. Provided that each liposome has an absolute charge greater than the polyplexes, and no excess DNA present, $\rho_N \geq 1$ ensures that all polyplexes are converted, and LPNPs are stable.

However intuitive, this $\rho_N \geq 1$ requirement is a critical insight. The reason why we and others have failed to think of it is because ρ_N is an elusive quantity, difficult to estimate beforehand or determine experimentally. Furthermore, it depends on sample preparation. Hence, ρ_N is not a salient feature in sample preparation and one tends to focus on absolute charge ratios instead. The latter are easier to control experimentally, but less useful in predicting the association between liposomes and polyplexes, since absolute charges are distributed over a discrete number of particles. FCCS then plays a crucial role in revealing and highlighting ρ_N by measuring both the number of polyplexes and liposomes simultaneously.

2.7. Polyplexes far from ρ_{iso} are more numerous, requiring more liposomes to form LPNPs.

Overall, $\rho_{\mathrm{P:DNA}} = 1$ polyplexes show similar trends to the $\rho_{\mathrm{P:DNA}} = 1.5$ system (Figures 2g and 2j). Namely, all the polyplexes are converted into LPNPs (f_{LPNP}≈1) and the average number of liposomes per LPNP (n) is also slightly greater than one, as seen from the A_X/A_R ratio slightly above one. However, there are two important additional points to highlight.

The first is that when significantly away from ρ_{iso}, some of the DNA is expected to remain free in solution, non-complexed[34]. This free DNA also needs to be complexed by the cationic liposomes for the system to become colloidally stable, thus requiring a larger $\rho_{\mathrm{L:DNA}}$ ratio. Liposomes complexed with this excess DNA are not expected to be associated with polyplexes, which explains the observation that A_X/A_G is measured at ca. 0.25. However, contrary to the $\rho_{\mathrm{P:DNA}} = 1.5$ case seen above, where a decreasing A_X/A_G is just indicative of superfluous liposomes, here, these extra liposomes are needed to neutralize free DNA, and almost certainly this indicates coexistence of LPNPs with lipoplexes. This partially explains the much larger $\rho_{\mathrm{L:DNA}}$ ratio needed to obtain stability in the $\rho_{\mathrm{P:DNA}} = 1$ systems.

The second is that the number of polyplexes is significantly greater for $\rho_{\mathrm{P:DNA}} = 1$ than $\rho_{\mathrm{P:DNA}} = 1.5$. This can be seen by the amplitudes of the green autocorrelation curves in Figures 2f and 2g (~5x greater – recall Eq 2a) and Table S5 (~3.5x greater). The greatest consequence of this larger number of polyplexes is that to ensure the $\rho_N \geq 1$ requirement, the number of liposomes needed to stabilize the system also increases. This, together with the excess of DNA discussed above, helps justifying the much higher $\rho_{\mathrm{L:DNA}}$ needed for $\rho_{\mathrm{P:DNA}} = 1$ LPNPs.

2.8. The amount of PEG on liposomes influences the number of liposomes per LPNP.

The findings above are largely reproduced when the 10 mol% PEG liposomes are replaced by 5 and 0 mol% PEG liposomes (Figure 3a). Both A_X/A_R and A_X/A_G ratios show similar trends across the three systems, indicating f_{LPNP}≈1 and n increasing slightly beyond one for large $\rho_{\mathrm{L:DNA}}$. However, it is also visible that as the PEG amount in the liposomes decreases, both the A_X/A_R and A_X/A_G ratios increase. This is more evident for A_X/A_G, since the A_X/A_R values have larger error bars. Overall, both these ratios indicate that while n is expected to still be relatively small, it increases when the PEGylation degree decreases. Since the PEG coating on liposomes acts as a steric barrier against adsorption, it is not surprising that on average low-PEG liposomes complex more extensively with polyplexes.

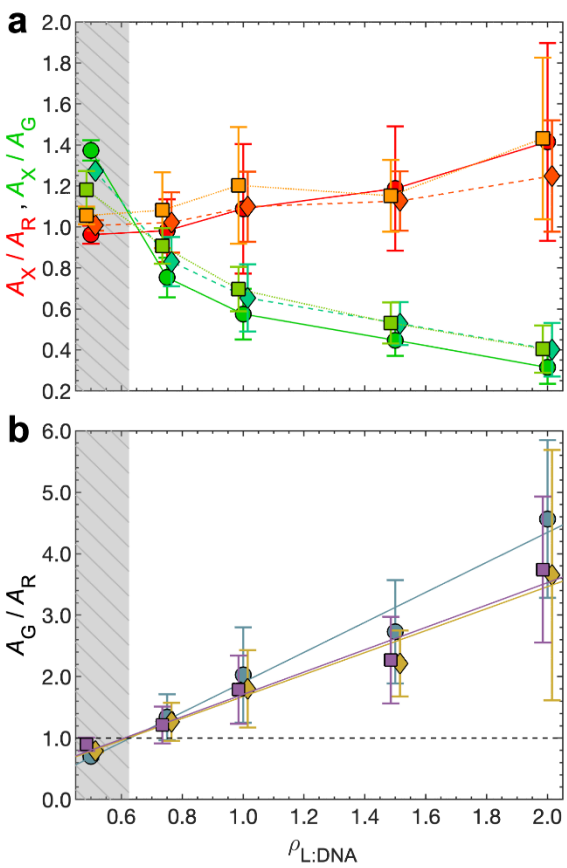

Figure 3. Effect of liposome PEGylation in the assembly of LPNPs. (**a**) A_X/A_R (red-orange symbols) and A_X/A_G (green-blue symbols) ratios for LPNP systems with 0 mol% PEG (squares), 5 mol% PEG (diamonds) and 10 mol% PEG (circles) liposomes. The trends are similar in the three systems, but there is a systematic small increase of the A_X/A_R and A_X/A_G pair for lower degrees of liposome PEGylation. This indicates that the conversion from polyplexes to LPNPs is practically complete for all three systems, but the fraction of used liposomes and average number of liposomes per LPNP increase slightly for lower degrees of liposome PEGylation. Note that similarly to Figures 2i-j, also here the A_X/A_R error bars are large, due to the quasi-single-particle nature of the measurements, but the mean values are robust and follow coherent trends. (**k**) A_G/A_R ratio for LPNP systems with 0 mol% PEG (squares), 5 mol% PEG (diamonds) and 10 mol% PEG (circles) liposomes. The trends are identical for the three systems. The regions of robust colloidal stability for LPNP formation show ρ_N>1, whereas the regions of marginal stability show ρ_N<1. The boundaries between marginal and robust stability (ρ_N=1) are the same for the three systems ($\rho_{\mathrm{L:DNA}}$=0.63). This reinforces that ρ_N≥1 is a requirement for robust stability. The fact that the linear fits to A_G/A_R have a lower slope for the 0 and 5 mol% PEG systems is caused by the

greater deviations to the 1:1 stoichiometry in these systems. Data in **a** and **b** is slightly offset in the horizontal axis for easier visualization. The grey-dashed areas delineate the compositions of marginal stability, in which some samples were not measurable due to the presence of aggregates. Data are Means ± SD (n≥3).

Regarding the ρ_N ratio, which is approximated by A_G/A_R (Figure 3b), also here we find $\rho_N > 1$ for all stable LPNPs, and $\rho_N < 1$ for the non-stable ones, which reinforces that $\rho_N \geq 1$ is a critical requirement for LPNP colloidal stability. The boundary between marginal and robust stability ($\rho_N = 1$) is similar for the three systems.

2.9. General features of LPNP assembly behaviour.

Figure 4 summarises the results and observations of this work in the form of a ternary map of assembly in excess water (given the out-of-equilibrium nature of the system, the map is not strictly a phase diagram). Additional details regarding the boundaries on the map and its implications are available in section S4.

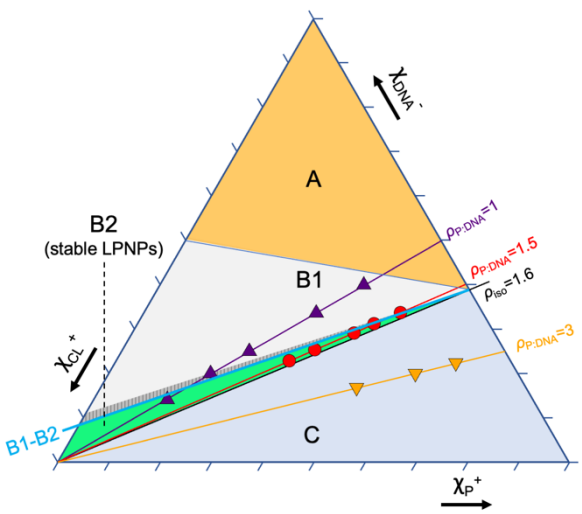

Figure 4. Ternary lipid-polylysine-DNA assembly map in excess water. The three axes represent the charge molar fractions of DNA (χ_{DNA^-}), polylysine (χ_{P^+}) and cationic liposomes (χ_{CL^+}). The polylysine concentration is fixed at 7 μg/mL. The map is subdivided in three main regions. Region A encompasses overall negatively charged systems (not investigated). In region B the starting polyplexes are negative but the overall charge is net-positive via addition of cationic liposomes. In sub-region B1 the assemblies are not colloidally-stable whereas in B2 LPNPs stable for at least one week are formed. The B1-B2 boundary between aggregation and stable LPNP formation is set by the liposome:polyplex ratio (ρ_N), which must be $\rho_N \geq 1$ when there is no excess DNA present (see text). The patterned area immediately above the B1-B2 boundary indicates the region where colloidal stability is observed only in some samples. The number of liposomes and polyplexes (hence ρ_N) is defined by both the composition and methodology. Within B2, $\rho_{P:DNA}$=1.5 LPNPs coexist with excess cationic liposomes, whereas $\rho_{P:DNA}$=1 LPNPs coexist with lipoplexes. In region C the starting polyplexes are positive (below the ρ_{iso} line), and no LPNP formation was observed after addition of cationic liposomes.

The first important observation is the lack of formation of LPNPs when starting with positive polyplexes (region C on the map). This indicates that the interaction between polylysine and DNA is robust, with the polycation not being displaced by liposomes. The second important observation is the need to have at least one liposome per polyplex ($\rho_N \geq 1$) to form stable LPNPs. This ensures that every polyplex is

enveloped by a liposome, having their negative charge reversed and inhibiting aggregation. This requirement divides region B into two subregions: B1, for $\rho_N < 1$, where aggregation is observed, and B2, for $\rho_N \geq 1$, where LPNPs stable for at least one week are formed. In B2, the conversion of polyplexes to LPNPs is complete, indicating that neither the polycation nor DNA are displaced by the liposomes.

While the location of the B1-B2 boundary is specific to this system, we postulate that the general features of LPNP assembly observed in this work can be transposed to systems containing reasonably strong polyelectrolytes and cationic liposomes with monovalent lipids and similar membrane rigidity. If weak polycations (with low ionization degree) are used in the formation of the polyplex cores, or multivalent cationic liposomes as the shell, enhanced lipid-DNA interactions in detriment of polycation-DNA could potentially lead to displacement of the polycation and modify the assembly behaviour. Regardless, the FCCS analysis approach detailed here can be extended to quantify the association between different components in complex systems and provide valuable insights into the overall assembly behaviour of LPNPs and other composite materials for diverse applications besides gene delivery.

Acknowledgements:

We are grateful to Cyrus Safinya (UCSB), Ulf Olsson (Lund U.) and Paulo Freitas (INL) for useful discussions. This research is supported by the Microfluidic Layer-by-layer Assembly of Cationic Liposome - Nucleic Acid Nanoparticles for Gene Delivery project (032520) co-funded by FCT and ERDF through COMPETE2020. JLP is supported by a post-doctoral fellowship from the Ramón Areces Foundation (reference BEVP30A5827).

Online content:

The supplementary data contains a detailed FCCS implementation description, 1:*n* polyplex:liposome stoichiometry model of LPNP formation, and determination of the overlap confocal volume.

3. MATERIALS AND METHODS

Materials:

The lipids 1,2-dioleoyl-3-trimethylammonium-propane (DOTAP), 1,2-dioleoyl-sn-glycero-3-phosphocholine (DOPC) and 1,2-distearoyl-sn-glycero-3-phosphoethanolamine-N-[amino(polyethylene glycol)-2000] (DSPE-PEG) solubilized in chloroform were purchased from Avanti Polar Lipids and used as received. Poly-L-lysine solution 0.1 % (w/v) in water was purchased from Sigma-Aldrich. GFP plasmid (pCMV-GFP), obtained through Addgene, was a gift from Connie Cepko (Addgene plasmid #11153)[49].

The dye Atto 488-NHS was purchased from ATTO-TEC GmbH. Texas Red 1,2-Dihexadecanoyl-snGlycero-3-Phosphoethanolamine, Triethylammonium salt (Texas Red-labelled lipid) and the dye YOYO-1 were purchased from ThermoFisher Scientific Inc. All the aqueous solutions were prepared with DNAse-free and RNAse-free MilliQ water.

Characterization techniques:

The different nanostructures obtained in this work were characterized by the following techniques: DLS and electrophoretic mobility ($\zeta_{\text{Potential}}$) were performed with a SZ-100 device from Horiba, measuring scattering at 173°. TEM of the samples after negative staining with UranyLess© (following the manufacturer´s instructions) was performed in a JEOL 2100 200kV TEM. FCCS was performed in a confocal microscope LSM780 from Zeiss following a previously described protocol[31], with 5 s per measurement and carrying out 40 repeats per sample (excitation laser lines: 488 nm for Atto 488 dye and 561 nm for Texas Red). Laser power was set so that the intensity in the "red" (561 nm) channel was slightly above that in the "green" (488 nm) channel, thus minimizing overestimation of cross-correlation due to crosstalk[46]. FCCS auto- and cross-correlation curves were fitted to a 3D normal diffusion model[50] using QuickFit 3.0 software and home-built Matlab scripts. After calibrating the FCCS setup employing fluorophores with a known diffusion coefficient[51], the fits obtained for the cross-correlation curves were used to obtain the diffusion coefficient of the LPNPs.

Labelling of polylysine with Atto 488 dye:

Polylysine was labelled by reacting the polymer with Atto 488-NHS (ratio 1:100 Atto dye: NH_2 groups in the polymer). After stirring in aqueous solution at room temperature overnight, the labelled polymer was obtained. The purification was performed by size exclusion chromatography using Sephadex G25® stationary phase.

Preparation of LPNPs:

Polyplexes were prepared by mixing aqueous solutions of plasmidic DNA and polylysine at different charge ratios (CR, ratio between positive charges in the polymer to negative charges in the plasmid: 1, 1.5 and 3), and incubating them at room temperature for 30 min in an orbital shaker.

PEGylated cationic liposomes (composition DOTAP/DOPC/DSPE-PEG 80/10/10) were prepared. First, the lipids were mixed in chloroform solution, followed by evaporation of the solvent, rehydration with water and sonication with a tip sonicator at a final total lipid concentration of 4 mM (sonication conditions:

10% amplitude, 1 minute, 50% duty cycle using a Branson Digital Sonifier® 250 Model). Cationic liposomes formulations with the ratios 80/15/5 and 80/20/0 were also prepared.

Finally, both components (polyplex and liposomes) were mixed at different proportions, with a lipid N/DNA P ratio in the range of 0.5-2. A final polylysine concentration of 7 μg/mL was fixed for all the prepared samples. The obtained dispersions were characterized by $\zeta_{\mathrm{Potential}}$ and DLS.

For FCCS, the LPNPs were prepared following the same protocol but employing labelled components. Atto 488-labeled polylysine was used to prepare the polyplexes, while Texas Red-labelled phospholipid was included in the liposomal formulation (0.2 % total lipid weight). Some samples were also prepared with YOYO 1-labeled DNA and Texas Red-labelled liposomes.

REFERENCES

1. Akinc, A. *et al.* The Onpattro story and the clinical translation of nanomedicines containing nucleic acid-based drugs. *Nature Nanotechnology* **14**, 1084–1087 (2019).
2. Polack, F. P. *et al.* Safety and Efficacy of the BNT162b2 mRNA Covid-19 Vaccine. *New England Journal of Medicine* **383**, 2603–2615 (2020).
3. Baden, L. R. *et al.* Efficacy and Safety of the mRNA-1273 SARS-CoV-2 Vaccine. *New England Journal of Medicine* **384**, 403–416 (2021).
4. Kranz, L. M. *et al.* Systemic RNA delivery to dendritic cells exploits antiviral defence for cancer immunotherapy. *Nature* **534**, 396–401 (2016).
5. Sahin, U. *et al.* Personalized RNA mutanome vaccines mobilize poly-specific therapeutic immunity against cancer. *Nature* **547**, 222–226 (2017).
6. Pastor, F. *et al.* An RNA toolbox for cancer immunotherapy. *Nature Reviews Drug Discovery* **17**, 751–767 (2018).
7. Gillmore, J. D. *et al.* CRISPR-Cas9 In Vivo Gene Editing for Transthyretin Amyloidosis. *New England Journal of Medicine* **385**, 493–502 (2021).

8. Rädler, J. O., Koltover, I., Salditt, T. & Safinya, C. R. Structure of DNA-cationic liposome complexes: DNA intercalation in multilamellar membranes in distinct interhelical packing regimes. *Science* **275**, 810–814 (1997).

9. Koltover, I., Salditt, T., Rädler, J. O. & Safinya, C. R. An Inverted Hexagonal Phase of Cationic Liposome-DNA Complexes Related to DNA Release and Delivery. *Science* **281**, 78–81 (1998).

10. Arteta, M. Y. *et al.* Successful reprogramming of cellular protein production through mRNA delivered by functionalized lipid nanoparticles. *Proceedings of the National Academy of Sciences* **115**, E3351–E3360 (2018).

11. Kulkarni, J. A. *et al.* On the Formation and Morphology of Lipid Nanoparticles Containing Ionizable Cationic Lipids and siRNA. *ACS Nano* **12**, 4787–4795 (2018).

12. Chaudhary, N., Weissman, D. & Whitehead, K. A. mRNA vaccines for infectious diseases: principles, delivery and clinical translation. *Nature Reviews Drug Discovery* **20**, 817–838 (2021).

13. Lorenzer, C., Dirin, M., Winkler, A.-M., Baumann, V. & Winkler, J. Going beyond the liver: Progress and challenges of targeted delivery of siRNA therapeutics. *Journal of Controlled Release* **203**, 1–15 (2015).

14. Degors, I. M. S., Wang, C., Rehman, Z. U. & Zuhorn, I. S. Carriers break barriers in drug delivery: endocytosis and endosomal escape of gene delivery vectors. *Accounts of Chemical Research* **52**, 1750–1760 (2019).

15. Ewert, K. K. *et al.* Cationic Liposomes as Vectors for Nucleic Acid and Hydrophobic Drug Therapeutics. *Pharmaceutics* **13**, 1365–1365 (2021).

16. Mitchell, M. J. *et al.* Engineering precision nanoparticles for drug delivery. *Nature Reviews Drug Discovery* **20**, 101–124 (2021).

17. Hyodo, M., Sakurai, Y., Akita, H. & Harashima, H. “Programmed packaging” for gene delivery. *Journal of Controlled Release* **193**, 316–323 (2014).

18. Wang, Y. & Huang, L. Composite Nanoparticles for Gene Delivery. in *Advances in Genetics* vol. 88 111–137 (Elsevier, 2014).

19. Caracciolo, G. *et al.* Factors Determining the Superior Performance of Lipid/DNA/Protammine Nanoparticles over Lipoplexes. *Journal of Medicinal Chemistry* **54**, 4160–4171 (2011).

20. Persano, S. *et al.* Lipopolyplex potentiates anti-tumor immunity of mRNA-based vaccination. *Biomaterials* **125**, 81–89 (2017).

21. Van der Jeught, K. *et al.* Dendritic Cell Targeting mRNA Lipopolyplexes Combine Strong Antitumor T-Cell Immunity with Improved Inflammatory Safety. *ACS Nano* **12**, 9815–9829 (2018).

22. Xue, Y. *et al.* A Synthetic Carrier of Nucleic Acids Structured as a Neutral Phospholipid Envelope Tightly Assembled on Polyplex Surface. *Advanced Healthcare Materials* **9**, 1901705–1901705 (2020).

23. Kaczmarek, J. C. *et al.* Optimization of a Degradable Polymer–Lipid Nanoparticle for Potent Systemic Delivery of mRNA to the Lung Endothelium and Immune Cells. *Nano Letters* **18**, 6449–6454 (2018).

24. Islam, M. A. *et al.* Restoration of tumour-growth suppression in vivo via systemic nanoparticle-mediated delivery of PTEN mRNA. *Nature Biomedical Engineering* **2**, 850–864 (2018).

25. Stadler, C. R. *et al.* Elimination of large tumors in mice by mRNA-encoded bispecific antibodies. *Nature Medicine* **23**, 815–817 (2017).

26. Lächelt, U. & Wagner, E. Nucleic Acid Therapeutics Using Polyplexes: A Journey of 50 Years (and Beyond). *Chemical Reviews* **115**, 11043–11078 (2015).

27. Schäfer, J., Höbel, S., Bakowsky, U. & Aigner, A. Liposome–polyethylenimine complexes for enhanced DNA and siRNA delivery. *Biomaterials* **31**, 6892–6900 (2010).

28. Chapel, J.-P. & Berret, J.-F. Versatile electrostatic assembly of nanoparticles and polyelectrolytes: Coating, clustering and layer-by-layer processes. *Current Opinion in Colloid & Interface Science* **17**, 97–105 (2012).

29. Siewert, C. D. *et al.* Hybrid Biopolymer and Lipid Nanoparticles with Improved Transfection Efficacy for mRNA. *Cells* **9**, 2034–2034 (2020).

30. Yan, J., Berezhnoy, N. V., Korolev, N., Su, C.-J. & Nordenskiöld, L. Structure and internal organization of overcharged cationic-lipid/peptide/DNA self-assembly complexes. *Biochimica et Biophysica Acta (BBA) - Biomembranes* **1818**, 1794–1800 (2012).

31. Bacia, K. & Schwille, P. Practical guidelines for dual-color fluorescence cross-correlation spectroscopy. *Nature Protocols* **2**, 2842–2856 (2007).

32. Peng, S. *et al.* Phase separation at the nanoscale quantified by dcFCCS. *Proceedings of the National Academy of Sciences of the United States of America* **117**, 27124–27131 (2020).

33. Gómez-Varela, A. I. *et al.* Fluorescence Cross-Correlation Spectroscopy as a valuable tool to characterize cationic liposome-DNA nanoparticle assembly. *Journal of Biophotonics* **14**, e202000200–e202000200 (2021).

34. Ketola, T. *et al.* Independent versus Cooperative Binding in Polyethylenimine − DNA. *J. Phys. Chem. B* **117**, 10405–10413 (2013).

35. Pigeon, L., Gonçalves, C., Pichon, C. & Midoux, P. Evidence for plasmid DNA exchange after polyplex mixing. *Soft Matter* **12**, 7012–7019 (2016).

36. Coelho, F., Botelho, C., Paris, J. L., Marques, E. F. & Silva, B. F. B. Influence of the media ionic strength on the formation and in vitro biological performance of polycation-DNA complexes. *Journal of Molecular Liquids* **344**, 117930–117930 (2021).

37. Weidemann, T. & Schwille, P. Dual-Color Fluorescence Cross-Correlation Spectroscopy with Continuous Laser Excitation in a Confocal Setup. in *Methods in Enzymology* vol. 518 43–70 (Elsevier, 2013).

38. Kim, S. A., Heinze, K. G. & Schwille, P. Fluorescence correlation spectroscopy in living cells. *Nature Methods* **4**, 963–973 (2007).

39. Yu, L. *et al.* A Comprehensive Review of Fluorescence Correlation Spectroscopy. *Frontiers in Physics* **9**, 644450–644450 (2021).

40. Merkle, D., Lees-Miller, S. P. & Cramb, D. T. Structure and dynamics of lipoplex formation examined using two-photon fluorescence cross-correlation spectroscopy. *Biochemistry* **43**, 7263–7272 (2004).

41. Berezhna, S. *et al.* New effects in polynucleotide release from cationic lipid carriers revealed by confocal imaging, fluorescence cross-correlation spectroscopy and single particle tracking. *Biochimica et Biophysica Acta (BBA) - Biomembranes* **1669**, 193–207 (2005).

42. Schaeffel, D. *et al.* Fluorescence correlation spectroscopy directly monitors coalescence during nanoparticle preparation. *Nano Letters* **12**, 6012–6017 (2012).

43. Cauda, V. *et al.* Colchicine-loaded lipid bilayer-coated 50 nm mesoporous nanoparticles efficiently induce microtubule depolymerization upon cell uptake. *Nano Letters* **10**, 2484–2492 (2010).

44. Ma, K., Zhang, D., Cong, Y. & Wiesner, U. Elucidating the Mechanism of Silica Nanoparticle PEGylation Processes Using Fluorescence Correlation Spectroscopies. *Chemistry of Materials* **28**, 1537–1545 (2016).

45. Wuttke, S. *et al.* MOF nanoparticles coated by lipid bilayers and their uptake by cancer cells. *Chemical Communications* **51**, 15752–15755 (2015).

46. Bacia, K., Petrášek, Z. & Schwille, P. Correcting for Spectral Cross-Talk in Dual-Color Fluorescence Cross-Correlation Spectroscopy. *ChemPhysChem* **13**, 1221–1231 (2012).

47. Werner, S., Ebenhan, J., Haupt, C. & Bacia, K. A Quantitative and Reliable Calibration Standard for Dual-Color Fluorescence Cross-Correlation Spectroscopy. *ChemPhysChem* **19**, 3436–3444 (2018).

48. Penacho, N., Filipe, A., Simões, S. & De Lima, M. C. P. Transferrin-associated lipoplexes as gene delivery systems: Relevance of mode of preparation and biophysical properties. *Journal of Membrane Biology* **221**, 141–152 (2008).

49. Matsuda, T. & Cepko, C. L. Electroporation and RNA interference in the rodent retina in vivo and in vitro. *Proc. Natl. Acad. Sci. U. S. A.* **101**, 16–22 (2004).

50. Krieger, J. W., Singh, A. P., Garbe, C. S., Wohland, T. & Langowski, J. Dual-Color Fluorescence Cross-Correlation Spectroscopy on a Single Plane Illumination Microscope (SPIM-FCCS). *Optics Express* **22**, 2358–2358 (2014).

51. Kapusta, P. Absolute Diffusion Coefficients: Compilation of Reference Data for FCS Calibration. *Application Note, PicoQuant GmbH* (2010).